Facile and Rapid Preparation of ZnO Nanomaterials with Different Morphologies and Superficial Structures for Enhanced Ethanol-Sensing Performances

Xiao-Xu Song, Huifen Fu, Xiangjie Li, Xiao-Hong Yi, Hong-Yu Chu & Chong-Chen Wang

Journal of Inorganic and Organometallic Polymers and Materials

ISSN 1574-1443
Volume 29
Number 1

J Inorg Organomet Polym (2019)
29:33-40
DOI 10.1007/s10904-018-0961-1

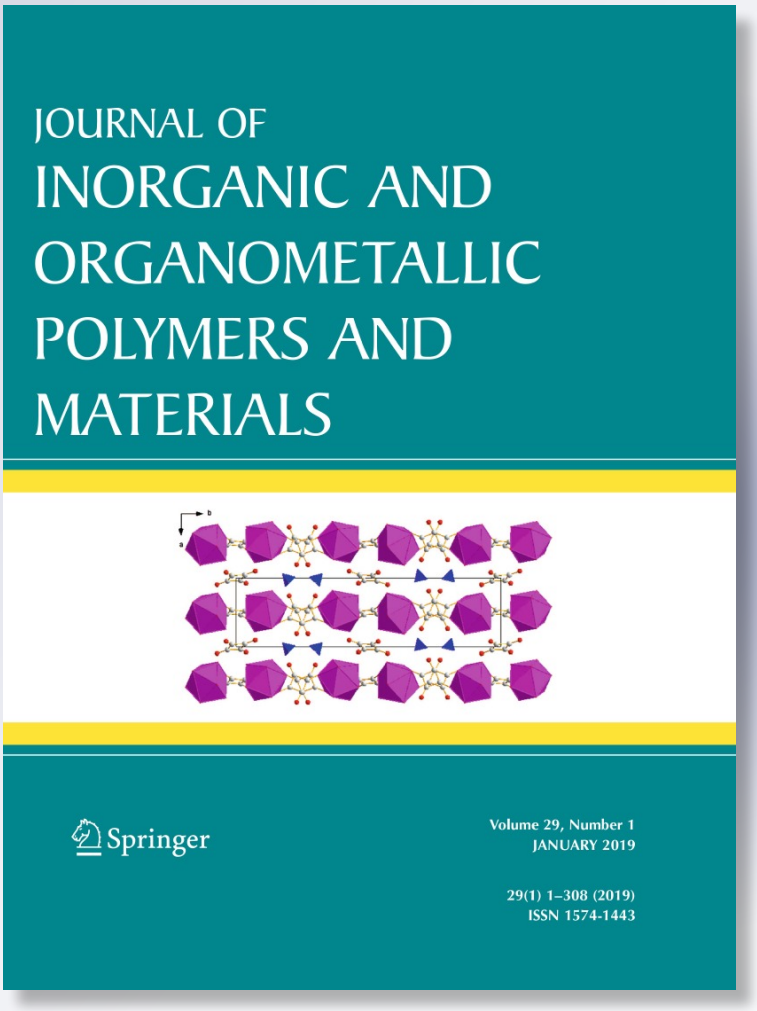

Springer

Journal of Inorganic and Organometallic Polymers and Materials (2019) 29:33–40
https://doi.org/10.1007/s10904-018-0961-1

Facile and Rapid Preparation of ZnO Nanomaterials with Different Morphologies and Superficial Structures for Enhanced Ethanol-Sensing Performances

Xiao-Xu Song[1] · Huifen Fu[1] · Xiangjie Li[1] · Xiao-Hong Yi[1] · Hong-Yu Chu[1] · Chong-Chen Wang[1]

Received: 23 July 2018 / Accepted: 3 September 2018 / Published online: 5 September 2018

Abstract
A facile, rapid and environmental-friendly method was developed to prepare ZnO with different morphologies and superficial structures just using $Zn(NO_3)_2$ and hexamethylenetetramine (HMTA) as precursors by tuning nucleation rate. Rod-like ZnO-1 and ZnO-5, and irregular ZnO-10 and ZnO-20 were obtained as the amounts of the used reagents are 1, 5, 10 and 20 mmol, respectively. Compared to ZnO-1, the responses of ZnO-5, ZnO-10 and ZnO-20 toward ethanol were improved greatly, which could be attributed to their alternative active adsorbed oxygen species (O^{2-}/O^- for ZnO-5, ZnO-10 and ZnO-20, O^{2-} for ZnO-1). It was proposed that the different active adsorbed oxygen species might result from the different activation of ethanol with the aid of ZnO. The response of ZnO-10 toward 50 ppm ethanol is 115, about five times higher than that of ZnO-1, and the best gas-sensing performance of ZnO-10 was deemed to result from its largest specific surface area and highest percentage of adsorbed oxygen.

Keywords ZnO · Nanomaterials · Gas sensor · Morphology · Active oxygen species

1 Introduction

ZnO, as a semiconductor metal oxide with low cost, non-toxic nature and good tunability, was widely used in many fields like gas sensor [1–4], catalysis [5, 6], luminescence [7, 8], solar cells [9, 10], etc. It is reported that ZnO responds well to toxic and hazard gases, such as ethanol [11–14], acetone [15–17], etc. However, gas-sensing performance of ZnO is required to be further improved to satisfy the practical applications. Morphology controlling is an important method to improve the gas-sensing performance [18]. Xue and co-workers prepared ZnO nanocone exposing highly active crystal facet that responded well to ethanol [19]. Currently, there are many methods have been reported to prepare different ZnO, in which nanorod [20], nanosheets [21], nanowires [21] and nanoflower [22] were successfully prepared. Some methods like hydrothermal, solvothermal, microwave-assisted synthesis, and so on, need high pressure that requires specific vessels, which is not conducive to industrial production. It is urgent to develop facile, rapid and environmental-friendly method to prepare ZnO to satisfy the practical applications.

Besides morphology controlling, regulating of superficial structures is also significant to the improving of the gas-sensing performance because the sensing mechanism of ZnO follows surface-controlled type [23, 24]. When ZnO is exposed to air, O_2 molecules will capture electrons from conductive band of ZnO to form adsorbed oxygen (O^{2-}, O^- and O^{2-}). Then, the detected gas will be firstly adsorbed and activated on the surface of ZnO, finally reacted with adsorbed oxygen, releasing electron to ZnO, causing change of resistant of ZnO. Therefore, regulating of adsorbed oxygen is always a hot topic in the field of gas sensor [25, 26]. In addition, the activation of targeted gas by ZnO can also affect the gas-sensing performance.

Within this paper, a facile, rapid and environmental-friendly method was developed to prepare ZnO with different morphologies and superficial structures by changing concentrations of $Zn(NO_3)_2$ and HMTA. The effects of morphology, specific surface area, percentage of adsorbed oxygen, type of active adsorbed oxygen specie and the activation

✉ Chong-Chen Wang
chongchenwang@126.com; wangchongchen@bucea.edu.cn

[1] Beijing Key Laboratory of Functional Materials for Building Structure and Environment Remediation, Beijing University of Civil Engineering and Architecture, Beijing 100044, China

of ethanol by ZnO on the ethanol-sensing performance were investigated. This study provides an effective method to improve gas-sensing performance of ZnO nanomaterials.

2 Experimental

2.1 Materials and Instruments

$Zn(NO_3)_2$ and hexamethylenetetramine (HMTA) were purchased from J&K Scientific Ltd, and used as received without further purification.

Morphologies of the samples were characterized using Hitachi HT7700 transmission electron microscopy (TEM) and SU8020 scanning electron microscopy (SEM). XRD patterns were recorded on a Dandonghaoyuan DX-2700B diffractometer using Cu Kα radiation in the range of $2\theta = 5°–90°$. Belsorp-mini II analyzer was used to characterize the specific surface areas of the samples. X-ray photoelectron spectra (XPS) were obtained using VG Scientific ESCALAB 250 spectrometer.

2.2 Preparation of ZnO with Different Morphologies

One millimole $Zn(NO_3)_2$ and 1 mmol HMTA were dissolved in 5 mL deionized water, respectively. 40 mL deionized water was added into a 100 mL flask, and heated to boiling at 100 °C. Then, the above $Zn(NO_3)_2$ and HMTA aqueous solution were added into the flask in turn. After 30 min, the obtained solution was allowed to cool down naturally. The product was separated by centrifugation (4500 rpm, 10 min), washed twice with deionized water and once with ethanol, and dried in a drying oven at 60 °C for 6 h. Then, the sample was calcined at 300 °C for 2 h with a warming rate of 5 °C/min using a pipe furnace, and the rod-like ZnO was obtained. This ZnO was renamed as ZnO-1 as the used amounts of $Zn(NO_3)_2$ and HMTA are 1 mmol. Using the similar method, ZnO-5, ZnO-10 and ZnO-20 were obtained as the added amounts of $Zn(NO_3)_2$ and HMTA are 5, 10 and 20 mmol, respectively.

2.3 Fabrication of the ZnO-Based Gas Sensor

Gas sensors were fabricated using ZnO-1, ZnO-5, ZnO-10 and ZnO-20 as gas-sensing materials. Briefly, ZnO and ethanol were mixed and grind into a paste in an agate mortar. The paste was coated on a ceramic tube with a pair of Au electrodes and four Pt wires, respectively. A Ni–Cr coil served as a heater to control the working temperature by tuning the heating current was inserted through the inner tube. Then, the ends of the Ni–Cr coil and Pt wires were welded to six electrodes of a pedestal, respectively, to form a gas sensor. The schematic illustration of the experimental procedure was shown in Fig. 1.

2.4 Gas-Sensing Measurement

The ZnO-based gas sensors were mounted on the CGS-8 gas sensor tester. After the heating current was set, the resistances of the ZnO-based gas sensor in air can be measured. R_a, the resistances of the ZnO-based gas sensors in air were obtained after the resistances were stable. When ethanol with a calculated volume was injected into the gas chamber using a syringe, the resistance decreased, and R_g, the resistance of the ZnO-based gas sensors in the target gas, was obtained after the resistance value was stable. The responses of the ZnO-based gas sensors for the reductive gas were

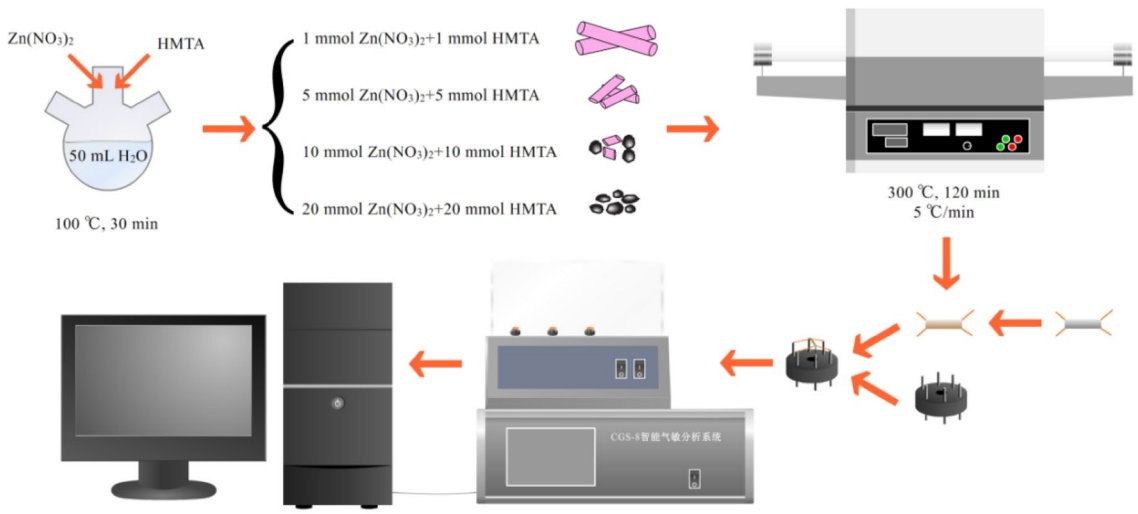

Fig. 1 Schematic illustration of the experimental procedure

defined as R_a/R_g. Subsequently, the gas chamber was opened, and the resistance was gradually restored to the initial value.

3 Results and Discussions

3.1 Characterization of ZnO Nanomaterials

ZnO can be obtained just reaction for 30 min under atmospheric pressure using $Zn(NO_3)_2$ and HMTA as precursors. During the preparation process, $Zn(NO_3)_2$ and HMTA are used, in which HMTA provides alkaline environment that is an important factor to form ZnO. Varying the amounts of $Zn(NO_3)_2$ and HMTA, ZnO with different morphologies are obtained (Fig. 2). It can be seen that ZnO-1 and ZnO-5 present rod-like shape, and both width and length of ZnO-1 are larger than those of ZnO-5 (Fig. 2a, b, e and f). Most ZnO-10 and ZnO-20 are irregular particles, and some small ZnO nanorods exist for ZnO-10 (Fig. 2c, d, g and h). The increasing of the amounts of $Zn(NO_3)_2$ and HMTA could accelerate the rate of nucleation, resulting in the changes of morphologies and sizes of ZnO. In a word, this method is not only facile, rapid and environmental-friendly, but also can achieve controllable regulating morphologies and sizes of ZnO.

All diffraction peaks in XRD patterns of the four samples can be well indexed to the hexagonal wurtzite structure (Fig. 3), and no characteristic peaks of impurities are observed. The sharp peaks of the samples indicate the good crystallinity of ZnO, and the differences of the relative intensities of (101), (100) and (002) crystal faces result from the different morphologies. According to the Scherrer equation ($D = \lambda/(\beta\cos\theta)$) where λ, β, θ and D is the wavelength of X-ray, the full width at half maximum of (101) peak of ZnO, the diffraction angel of the (101) peak and the grain size of ZnO, respectively, the calculated D for the ZnO-1, ZnO-5, ZnO-10 and ZnO-20 is 31.2, 31.2, 26.9 and 28.8 nm, respectively. Small grain size facilitates the electron transformation and the increase of the specific surface area, leading to the improvement of the gas-sensing performance.

3.2 Ethanol-Sensing Performances

Gas-sensing performances are evaluated using CGS-8 gas sensor tester. The changes of the resistances are used to detect the targeted gas, and the response is defined as R_a/R_g, in which the R_a and R_g are the resistances of ZnO in air and ethanol, respectively. Figure 4a shows that the responses of the four ZnO to 50 ppm ethanol firstly increase, then decrease with the increasing of the optimal working temperature, and reach the highest at 190 °C. In general, ethanol is firstly adsorbed and activated on the surface of ZnO, and then reacted with adsorbed oxygen, leading to the electron transfer and resistance changes of ZnO. When the working temperature is too low, the adsorption and activation of the ethanol molecule on the surface of ZnO are not sufficient to overcome energy barrier to react with the adsorbed oxygen. However, the adsorbed ethanol would be desorbed from the surface of ZnO when the working temperature exceeds the optimum one, which would cause a lower response. It can be observed from Fig. 4a that the responses of ZnO-5, ZnO-10 and ZnO-20 are improved greatly compared to ZnO-1. ZnO-10 has the highest response among the four samples, followed by ZnO-20, ZnO-5 and ZnO-1, and the responses to 50 ppm ethanol at 190 °C for the four samples are 115, 107, 78 and 20.5, respectively. The response of ZnO-10 toward 50 ppm ethanol is about five times higher than that of ZnO-1, indicating that it is an effective method to improve the gas-sensing performance by tuning the nucleation rate. The response-recovery curves to 50 ppm ethanol of these four samples are showed in Fig. 4b, and it can be seen that the four samples have satisfied response time and recovery time.

Figure 4c shows the responses of these four ZnO to ethanol in the concentration range 5–100 ppm. It can be observed that the corresponding responses of these ZnO improve with the increase of the concentration, and the enhancing of the response slows down gradually. These results correspond well with that reported in literatures [27]. Compared to the ethanol gas-sensing materials reported in literatures (Table 1) [14, 19, 28–36], ZnO-10 has higher response and lower working temperature.

The gas adsorption model of semiconductor empirically described as Eq. (1) [23, 37].

$$S_g = 1 + A_g(C_g)^{\beta} \tag{1}$$

where S_g is the sensitivity, C_g is the gas concentration, A_g is a prefactor, and β is a exponent on P_g. Generally, β has an ideal value of either 0.5 or 1, which depends on the reaction between superficial adsorbed oxygen and targeted gas. It is reported that the adsorbed oxygen species is O^{2-} when β is 0.5, while O^- when β is 1. Equation (1) can be rewritten in logarithmic form as Eq. (2).

$$\log(S_g - 1) = A_g + \beta \log C_g \tag{2}$$

There is a liner relationship between $\log(S_g - 1)$ and $\log C_g$, and the slope is β. In our case, the liner relationship is good for all the ZnO nanomaterials. The inset of the Fig. 4c presents that the values of β are 0.5335, 0.7759, 0.8301 and 0.8583 for ZnO-1, ZnO-5, ZnO-10 and ZnO-20, respectively, revealing that the active adsorbed oxygen specie is mainly O^{2-} for ZnO-1, while are O^{2-} and O^- for ZnO-5, ZnO-10 and ZnO-20, which could account for the great improvement of gas-sensing performance for the later three samples compared to ZnO-1. This proves that changing concentrations of $Zn(NO_3)_2$ and HMTA can regulate the

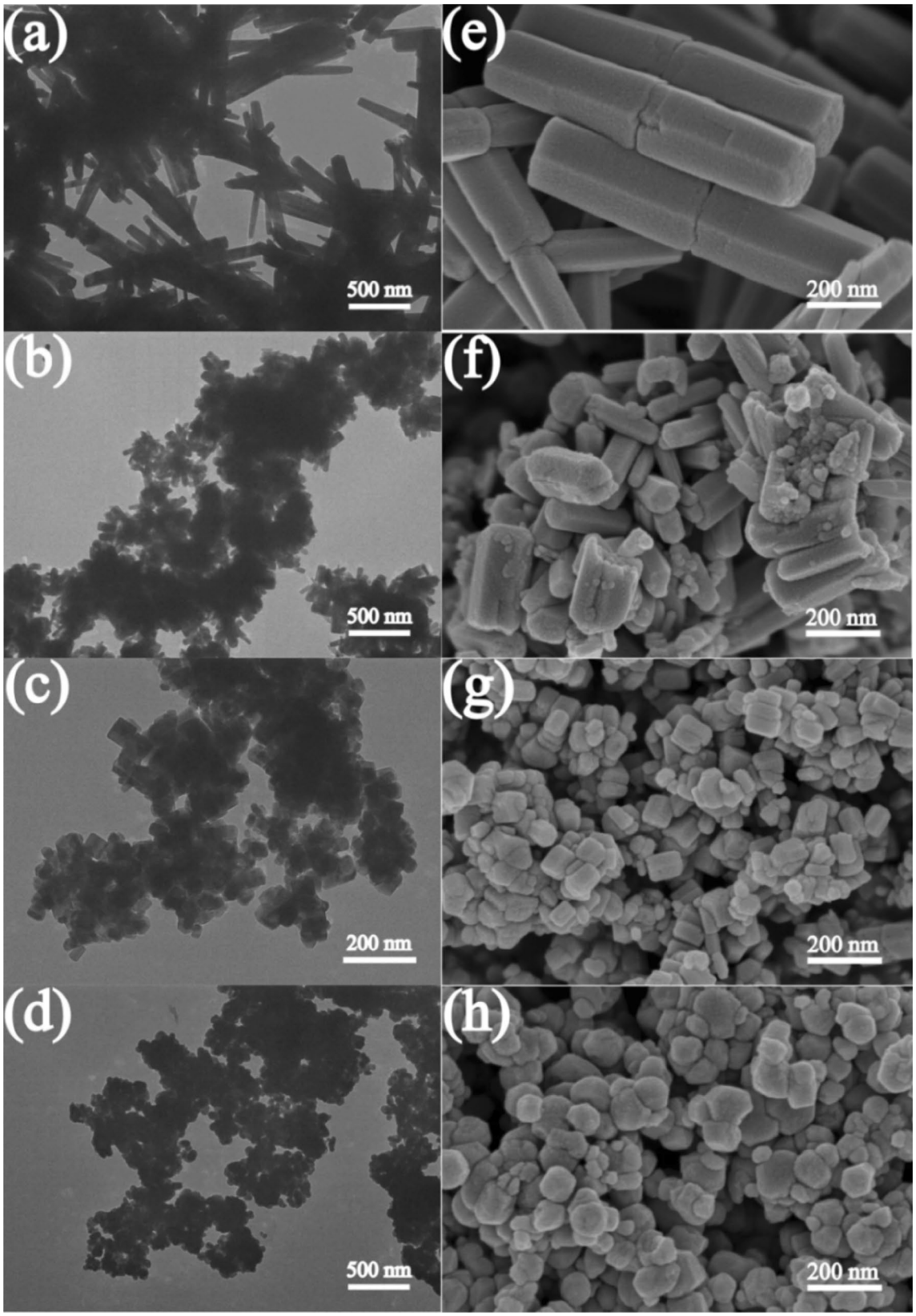

Fig. 2 **a**–**d** TEM and **e**–**h** SEM images of **a, e** ZnO-1, **b, f** ZnO-5, **c, g** ZnO-10 and **d, h** ZnO-20 annealed at 300 °C

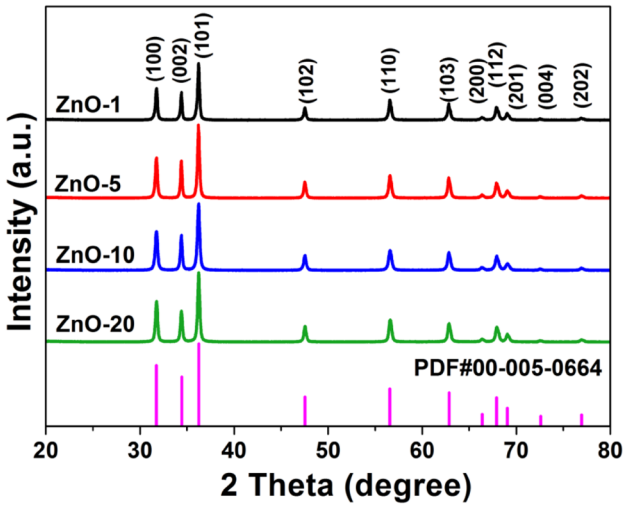

Fig. 3 XRD patterns of the four ZnO annealed at 300 °C

active adsorbed oxygen species which are vital to improve the gas-sensing performance.

Figure 4d shows that all samples have excellent repeatability and stability. When ethanol is pumped in, the resistance changes immediately and the response increases rapidly. Once ethanol is pumped out, ethanol can be removed from the surface of ZnO, and the resistance goes back to the initial value quickly, favoring the next measurement. Selectivity is an important factor to evaluate the gas-sensing performance. As shown in Fig. 5, the responses to different toxic gases were measured, including acetone, methanol, isopropanol formaldehyde, n-hexane and ammonia, and the responses of these ZnO to ethanol are much higher than those of other toxic gases, indicating the satisfied selectivity.

3.3 Reasons for the Difference of the Gas-Sensing Performance

To clarify the different gas-sensing performance of these four ZnO nanomaterials, nitrogen adsorption–desorption isotherms were carried out, and the results are shown in Fig. 6 and Table 2. It can be found that ZnO-10 has the largest specific surface areas, followed by ZnO-20, ZnO-5 and ZnO-1, which corresponds well with the gas-sensing performance. Larger specific surface areas provide more active sites, facilitating the improvement of gas-sensing performance. The difference of the specific surface area resulted

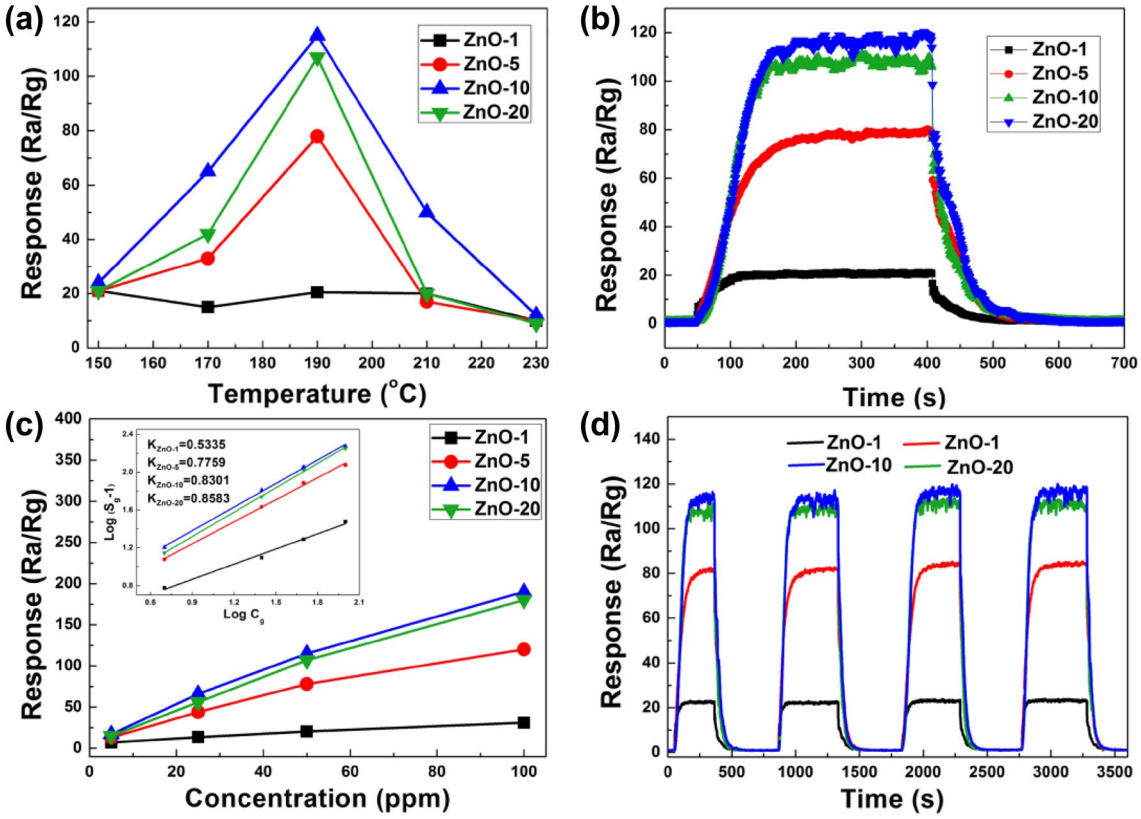

Fig. 4 **a** Responses of ZnO-1, ZnO-5, ZnO-10 and ZnO-20–50 ppm ethanol at different working temperature, **b** Response-recovery curves to 50 ppm ethanol of these samples, **c** Response versus gas concentration curves of these samples in the range of 1–100 ppm, and the inset is the corresponding $\log(S_g - 1)$ versus $\log C_g$, **d** Cycle tests of the four samples to 50 ppm ethanol

Table 1 Comparison of ethanol-sensing performances of sensing materials previously reported in literatures

Sensing materials	Concentration (ppm)	Response (R_a/R_g)	Working temperature (°C)	References
ZnO nanoparticles	100	190	190	This work
ZnO nanoparticles	50	115	190	This work
ZnO nanoparticles	25	66	190	This work
ZnO nanopyramid	100	43.2	225	[19]
5 at% In-doped 3DOM ZnO	100	88	250	[28]
ZnO nanosheets decorated with CuO nanoparticles	200	130	320	[29]
ZnO/SnO_2 hollow sphere	30	34.8	225	[30]
0.5 wt% Au loaded 3DOM In_2O_3	100	205	230	[31]
Er doped In_2O_3 hollow sphere	100	40.3	215	[32]
ZnO long nanofibers	100	51	270	[33]
ZnO nanorod	50	21	320	[14]
Al-doped NiO nanorod-flower	100	12	200	[34]
In_2O_3 nanorod decorated with Bi_2O_3 nanoparticle	200	17.7	200	[35]
Mesoporous Bi_2WO_4	100	34.6	300	[36]

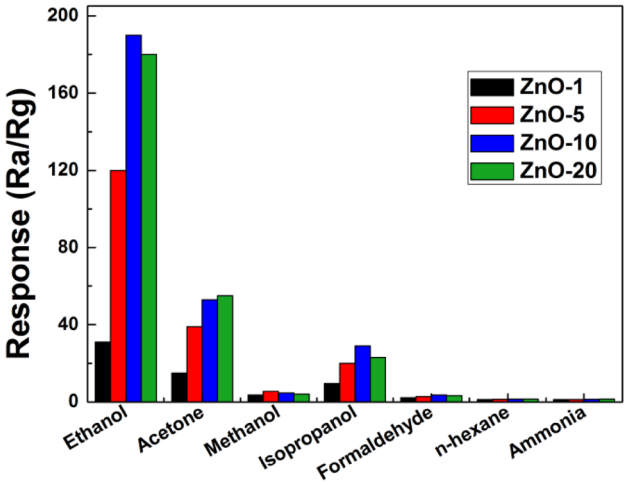

Fig. 5 Selectivity of ZnO-1, ZnO-5, ZnO-10 and ZnO-20–100 ppm different toxic gases

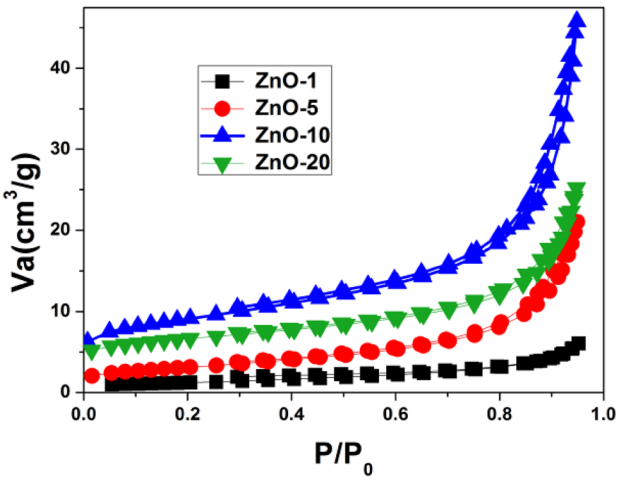

Fig. 6 Nitrogen adsorption–desorption isotherms of ZnO-1, ZnO-5, ZnO-10 and ZnO-20

from the particle size (evidenced by TEM and SEM) and grain size (evidenced by XRD). It can be seen from TEM and SEM that the ZnO-1 has the largest particle size, followed by the ZnO-5, ZnO-10 and ZnO-20. Although the particle sizes of the ZnO-10 and ZnO-20 are similar, particle aggregation of the ZnO-20 can be observed. The grain size calculated from XRD for the ZnO-1, ZnO-5, ZnO-10 and ZnO-20 is 31.2, 31.2, 26.9 and 28.8 nm, respectively. As is known to us, smaller grain size facilitates the appearance of pores and the increase of the specific surface area. Therefore, the ZnO-10 has the largest specific surface area, followed by the ZnO-20, ZnO-5 and ZnO-1.

Adsorbed oxygen is significant to improve the gas-sensing performance, therefore XPS spectra was used to measure

Table 2 Specific surface areas of ZnO-1, ZnO-5, ZnO-10 and ZnO-20

Samples	S_a (m^2/g)
ZnO-1	4.3
ZnO-5	10.5
ZnO-10	20.9
ZnO-20	12.3

the percentages of superficial oxygen species. Figure 7 shows that the O1s peaks of the four samples varies from each other, and the O1s peak can be consistently fitted by two Gaussian curves, centered at about 530.0 and 531.6 eV, respectively. The peak on the low binding energy side can be assigned to lattice oxygen (OI), and the other peak belongs

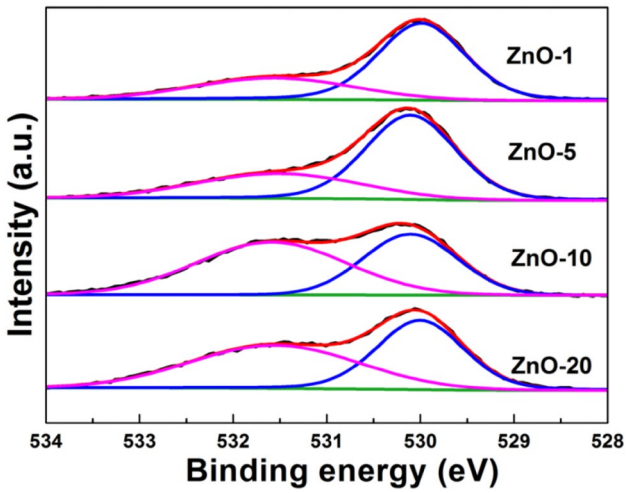

Fig. 7 O1s XPS spectra of ZnO-1, ZnO-5, ZnO-10 and ZnO-20

Table 3 Comparison of relative amount of oxygen species for ZnO-1, ZnO-5, ZnO-10 and ZnO-20 obtained from O1s XPS spectra

Samples	OI		OII	
	Peak (eV)	Percentage (%)	Peak (eV)	Percentage (%)
ZnO-1	530.0	68.7	531.6	31.3
ZnO-5	530.1	66.8	531.5	33.2
ZnO-10	530.1	42.0	531.6	58.0
ZnO-20	530.0	47.3	531.6	52.7

to adsorbed oxygen (OII) [38, 39]. Table 3 exhibits that ZnO-10 has the largest percentage of OII, followed by ZnO-20, ZnO-5 and ZnO-1, which also corresponds well with the gas-sensing performance. The main oxygen species (> 50%) are OII for ZnO-10 and ZnO-20, which can account for the better ethanol-sensing performance compared to ZnO-1 and ZnO-5. When the concentrations of $Zn(NO_3)_2$ and HMTA are increased, the growth rate of ZnO will be enhanced, leading to the formation of superficial defects which facilitate the formation of adsorbed oxygen. It is worthy to note that the difference of OII percentages for ZnO-1 and ZnO-5 is litter (31.3% for ZnO-1 and 33.3% for ZnO-5), and the specific surface area of ZnO-5 is as two times as that of ZnO-1, but the response of ZnO-5 is as four times as ZnO-1, which could be resulted from the difference of the active adsorbed oxygen species (O^{2-} for ZnO-1, O^{2-} and O^{-} for ZnO-5, as proved above). In addition, although the ZnO-5 and ZnO-20 have similar specific surface area and active adsorbed oxygen species, the larger percentage of OII for the ZnO-20 leads to the better gas-sensing performance. ZnO-10 possesses the largest specific surface area and percentage of OII, and the active adsorbed oxygen specie is O^{-} and O^{2-}, leading to the fivefold enhanced response compared to ZnO-1. Therefore, it can be concluded from the above discussion that specific surface area, the active oxygen specie and the percentage of OII are the dominant factors for the improving of the gas-sensing performance.

The gas-sensing mechanism of ZnO, as an n-type semiconductor, follows surface-controlled type. When ZnO is exposed to air, O_2 molecules will capture electrons from conduction band of ZnO to form adsorbed oxygen (O_2^{-}, O^{-} and O^{2-}), as described in Eqs. (3–5), resulting in the formation of thick electron depletion with high resistance [19, 28].

$$O_{2(air)} + e^{-} = O_{2(ads)}^{-} \quad (3)$$

$$O_{2(ads)}^{-} + e^{-} = 2O_{(ads)}^{-} \quad (4)$$

$$O_{(ads)}^{-} + e^{-} = O_{(ads)}^{2-} \quad (5)$$

When ethanol, a reductive gas, is injected in, ethanol molecules will be firstly adsorbed and then activated on the surface of ZnO, finally reacted with adsorbed oxygen, releasing electron to ZnO, leading to thinner electron depletion with lower resistance. The sensing reaction can be expressed by Eq. (6) for ZnO-1, while Eqs. (6) and (7) for ZnO-5, ZnO-10 and ZnO-20 as the active adsorbed oxygen specie is O^{2-} for the former sample, and O^{-} and O^{2-} for the later three samples [40, 41].

$$CH_3CH_2OH_{(ads)} + 6O_{(ads)}^{2-} = 2CO_2(g) + 3H_2O(l) + 12e^{-} \quad (6)$$

$$CH_3CH_2OH_{(ads)} + 12O_{(ads)}^{-} = 2CO_2(g) + 3H_2O(l) + 12e^{-} \quad (7)$$

It can be speculated from the Eqs. (3–5) that O^{-} and O^{2-} could exist on the surfaces of ZnO. Generally, O^{2-} is unstable and energetic than O^{-}, therefore O^{2-} can react with ethanol adsorbed on the surface of ZnO for all the samples. However, O^{-} can just react with the adsorbed ethanol for ZnO-5, ZnO-10 and ZnO-20, which may be caused from that the activation of ethanol is more efficient for the three samples compared to ZnO-1.

4 Conclusion

In summary, rod-like and irregular ZnO nanomaterials were prepared under atmospheric pressure at 100 °C with low and high concentrations of $Zn(NO_3)_2$ and HMTA, respectively, due to the alteration of the nucleation rate. Compared to ZnO-1, the gas-sensing performance is improved greatly for ZnO-5, ZnO-10 and ZnO-20 because the active adsorbed oxygen species are O^{2-} and O^{-} for the later three samples, while is O^{2-} for the former one, which might cause from the different activation of ethanol by these ZnO. ZnO-10 has the

largest response, followed by ZnO-20, ZnO-5 and ZnO-1, which is contributed to the discrepancies of specific surface areas, percentage of adsorbed oxygen and active adsorbed oxygen species. The response of ZnO-10 toward 50 ppm ethanol is 115, about five times higher than that of ZnO-1. This study can provide an effective method to improve the gas-sensing performance of ZnO nanomaterials.

Acknowledgements This work was supported by the National Natural Science Foundation of China (51578034), Beijing Postdoctoral Research Foundation, Great Wall Scholars Training Program Project of Beijing Municipality Universities (CIT&TCD20180323), Project of Construction of Innovation Teams and Teacher Career Development for Universities and Colleges Under Beijing Municipality (IDHT20170508), Beijing Talent Project (2017A38), Scientific Research Foundation of Beijing University of Civil Engineering and Architecture (KYJJ2017008), and the Fundamental Research Funds for Beijing University of Civil Engineering and Architecture (X18276).

References

1. L. Zhu, W. Zeng, Sens. Actuator A-Phys. **267**, 242–261 (2017)
2. J.-W. Kim, Y. Porte, K.Y. Ko, H. Kim, J.-M. Myoung, ACS Appl. Mater. Interfaces **9**, 32876–32886 (2017)
3. T. Wu, Z. Wang, M. Tian, J. Miao, H. Zhang, J. Sun, Sens. Actuator. B-Chem. **259**, 526–531 (2018)
4. B.L. Zhu, C.S. Xie, A.H. Wang, J. Wu, R. Wu, J. Liu, J. Mater. Sci. **42**, 5416–5420 (2007)
5. X. Liu, M.-H. Liu, Y.-C. Luo, C.-Y. Mou, S.D. Lin, H. Cheng, J.-M. Chen, J.-F. Lee, T.-S. Lin, J. Am. Chem. Soc. **134**, 10251–10258 (2012)
6. D.D. Thongam, J. Gupta, N.K. Sahu, D. Bahadur, J. Mater. Sci. **53**, 1110–1122 (2018)
7. H.-M. Xiong, Y. Xu, Q.-G. Ren, Y.-Y. Xia, J. Am. Chem. Soc. **130**, 7522–7523 (2008)
8. H.-M. Xiong, J. Mater. Chem. **20**, 4251–4262 (2010)
9. A.B.F. Martinson, J.W. Elam, J.T. Hupp, M.J. Pellin, Nano Lett. **7**, 2183–2187 (2007)
10. R. Kumar, A. Umar, G. Kumar, H.S. Nalwa, A. Kumar, M.S. Akhta, J. Mater. Sci. **52**, 4743–4795 (2017)
11. Z. Xue, Z. Cheng, J. Xu, Q. Xiang, X. Wang, J. Xu, ACS Appl. Mater. Interfaces **9**, 41559–41567 (2017)
12. B. Wang, T. Shi, W. Zhu, G. Liao, X. Li, J. Huang, T. Zhou, Z. Tang, Sens. Actuator. B-Chem. **245**, 821–827 (2017)
13. N.L. Tarwal, A.V. Rajgure, J.Y. Patil, M.S. Khandekar, S.S. Suryavanshi, P.S. Patil, M.G. Gang, J.H. Kim, J.H. Jang, J. Mater. Sci. **48**, 7274–7282 (2013)
14. L. Wang, Y. Kang, X. Liu, S. Zhang, W. Huang, S. Wang, Sens. Actuator. B-Chem. **162**, 237–243 (2012)
15. P.P. Sahay, J. Mater. Sci. **40**, 4383–4385 (2005)
16. S.-M. Li, L.-X. Zhang, M.-Y. Zhu, G.-J. Ji, L.-X. Zhao, J. Yin, L.-J. Bie, Sens. Actuator. B-Chem. **249**, 611–623 (2017)
17. M.R. Alenezi, S.J. Henley, N.G. Emerson, S.R.P. Silva, Nanoscale **6**, 235–247 (2014)
18. F. Yang, Z. Guo, J. Colloid Interface Sci. **462**, 140–147 (2016)
19. Z. Wang, J. Xue, D. Han, F. Gu, ACS Appl. Mater. Inter. **7**, 308–317 (2015)
20. J. Qi, J. Chang, X. Han, R. Zhong, M. Jiang, Z. Chen, B. Liu, Mater. Chem. Phys. **211**, 168–171 (2018)
21. M.-H. Jung, M.-J. Chu, J. Mater. Chem. C **2**, 6675–6682 (2014)
22. F. Xie, A. Centeno, B. Zou, M.P. Ryan, D.J. Riley, N.M. Alford, J. Colloid Interface. Sci. **395**, 85–90 (2013)
23. Y. Shi, M. Wang, C. Hong, Z. Yang, J. Deng, X. Song, L. Wang, J. Shao, H. Liu, Y. Ding, Sens. Actuator B-Chem. **177**, 1027–1034 (2013)
24. A. Yu, J. Qian, H. Pan, Y. Cui, M. Xu, Q. Chai, X. Zhou, Sens. Actuator B-Chem. **158**, 9–16 (2011)
25. F. Gu, D. You, Z. Wang, D. Han, G. Guo, Sens. Actuator B-Chem. **204**, 342–350 (2014)
26. F. Gu, L. Zhang, Z. Wang, D. Han, G. Guo, Sens. Actuator B-Chem. **193**, 669–678 (2014)
27. J. Qi, K. Chen, Y. Xing, H. Fan, H. Zhao, J. Yang, L. Li, B. Yan, J. Zhou, L. Guo, S. Yang, Nanoscale **10**, 7440–7450 (2018)
28. Z. Wang, Z. Tian, D. Han, F. Gu, ACS Appl. Mater. Interfaces **8**, 5466–5474 (2016)
29. X. Liu, Y. Sun, M. Yu, Y. Yin, B. Du, W. Tang, T. Jiang, B. Yang, W. Cao, M.N.R. Ashfold, Sens. Actuator B-Chem. **255**, 3384–3390 (2018)
30. J. Liu, T. Wang, B. Wang, P. Sun, Q. Yang, X. Liang, H. Song, G. Lu, Sens. Actuator B-Chem. **245**, 551–559 (2017)
31. F. Gu, R. Nie, Z. Tian, D. Han, Z. Wang, RSC Adv. **5**, 99018–99022 (2015)
32. T. Zhang, F. Gu, D. Han, Z. Wang, G. Guo, Sens. Actuator B-Chem. **177**, 1180–1188 (2013)
33. S. Wei, S. Wang, Y. Zhang, M. Zhou, Sens. Actuator B-Chem. **192**, 480–487 (2014)
34. C. Wang, X. Cui, J. Liu, X. Zhou, X. Cheng, P. Sun, X. Hu, X. Li, J. Zheng, G. Lu, ACS Sens. **1**, 131–136 (2015) (2016)
35. S. Park, S. Kim, G.J. Sun, C. Lee, ACS Appl. Mater. Interfaces **7**, 8138–8146 (2015)
36. D. Wang, Y. Zhen, G. Xue, F. Fu, X. Liu, D. Li, J. Mater. Chem. C **1**, 4153–4162 (2013)
37. T. Chen, H.-I. Chen, C.-S. Hsu, C.-C. Huang, J.-S. Wu, P.-C. Chou, W.-C. Liu, Sens. Actuator B-Chem. **221**, 491–498 (2015)
38. H.B. Huang, D.Y.C. Leung, D.Q. Ye, J. Mater. Chem. **21**, 9647–9652 (2011)
39. X.W. Li, X. Zhou, H. Guo, C. Wang, J.Y. Liu, P. Sun, F.M. Liu, G. Lu, ACS Appl. Mater. Interfaces **6**, 18661–18667 (2014)
40. B. Gong, T. Shi, G. Liao, X. Li, J. Huang, T. Zhou, Z. Tang, Sens. Actuator. B-Chem. **245**, 821–827 (2017)
41. S. Choi, M. Bonyani, G.-J. Sun, J.K. Lee, S.K. Hyun, C. Lee, Appl. Surf. Sci. **432**, 241–249 (2018)